HAL open science

Two-Dimensional Electron Gas at Spinel/Perovskite Interface: Suppression of Polar Catastrophe by an Ultrathin Layer of Interfacial Defects

Junfeng Ding, Jianli Cheng, Fatih Dogan, Yangyang Li, Weinan Lin, Yinbang Yao, Aurelien Manchon, Kesong Yang, Tom Wu

To cite this version:

Junfeng Ding, Jianli Cheng, Fatih Dogan, Yangyang Li, Weinan Lin, et al.. Two-Dimensional Electron Gas at Spinel/Perovskite Interface: Suppression of Polar Catastrophe by an Ultrathin Layer of Interfacial Defects. ACS Applied Materials & Interfaces, 2020, 12 (38), pp.42982-42991. 10.1021/acsami.0c13337 . hal-03036252

HAL Id: hal-03036252

https://hal.science/hal-03036252v1

Submitted on 2 Dec 2020

HAL is a multi-disciplinary open access archive for the deposit and dissemination of scientific research documents, whether they are published or not. The documents may come from teaching and research institutions in France or abroad, or from public or private research centers.

L'archive ouverte pluridisciplinaire **HAL**, est destinée au dépôt et à la diffusion de documents scientifiques de niveau recherche, publiés ou non, émanant des établissements d'enseignement et de recherche français ou étrangers, des laboratoires publics ou privés.

Distributed under a Creative Commons Attribution - NonCommercial - NoDerivatives 4.0 International License

Two-Dimensional Electron Gas at Spinel/Perovskite Interface: Suppression of Polar Catastrophe by an Ultrathin Layer of Interfacial Defects

Junfeng Ding,[1] *Jianli Cheng*,[2] *Fatih Dogan*,[3] *Yangyang Li*,[3] *Weinan Lin*,[4] *Yinbang Yao*,[5] *Aurelien Manchon*,[6] *Kesong Yang*,[2]* *and Tom Wu*[7]*

[1]Key Laboratory of Materials Physics, Institute of Solid State Physics, Chinese Academy of Sciences, Hefei 230031, People's Republic of China

[2]Department of NanoEngineering, University of California, San Diego, La Jolla, CA 92093-0448, USA

[3]College of Engineering and Technology, American University of the Middle East, Kuwait

[4]Department of materials science and engineering, National University of Singapore, Singapore

[5]School of Material and Energy, Guangdong University of Technology, Guangzhou 510006, People's Republic of China

[6]Physical Science and Engineering Division, King Abdullah University of Science and Technology, Thuwal, 23955-6900, Kingdom of Saudi Arabia

[7]School of Materials Science and Engineering, University of New South Wales (UNSW), Sydney, NSW 2052, Australia

ABSTRACT: Two-dimensional electron gas (2DEG) at the interface between two insulating perovskite oxides has attracted much interest for both fundamental physics and potential applications. Here, we report the discovery of a new 2DEG formed at the interface between spinel $MgAl_2O_4$ and perovskite $SrTiO_3$. Transport measurements, electron microscopy imaging and first-principles calculations reveal that the interfacial 2DEG is closely related to the symmetry breaking at the $MgAl_2O_4/SrTiO_3$ interface. The critical film thickness for the insulator-to-metal transition is approximately 32 Å, which is twice as thick as that reported on the widely studied $LaAlO_3/SrTiO_3$ system. Scanning transmission electron microscopy imaging indicates the formation of interfacial Ti-Al antisite defects with a thickness of ~4 Å. First-principles density functional theory calculations indicate that the co-existence of the antisite defects and surface oxygen vacancies may explain the formation of interfacial 2DEG as well as the observed critical film thickness. The discovery of 2DEG at the spinel/perovskite interface introduces a new material platform for designing oxide interfaces with desired characteristics.

KEYWORDS: oxide interface, two-dimensional electron gas, spinel, perovskite, titanium oxides

1. INTRODUCTION

Interfacial engineering between oxides, taking advantage of advanced material fabrication techniques with layer-by-layer control in heterostructures, provides new opportunities in oxide electronics to explore novel phenomena through breaking the translation or inversion symmetry at the interface.[1-4] One prominent example is the discovery of two-dimensional electron gas (2DEG) with extremely high charge carrier mobility at the interface of two band-insulators, $LaAlO_3$ (LAO) and $SrTiO_3$ (STO).[5-8] The LAO/STO interface also exhibits other fantastic properties not present in conventional semiconductor heterostructures, such as superconductivity,[9] magnetism,[10] and electronic phase separation.[11] Thus, the interfacial 2DEG has become a focal point for the application of oxide electronics.[12]

Although a large amount of experimental and theoretical work has been performed, the origin of the 2DEG at LAO/STO interfaces is still under debate.[13-15] In the earlier studies, the polar catastrophe at the LAO/STO interfaces is suggest to be responsible for the interfacial 2DEG.[5, 13, 16] The symmetry breaking at the $(LaO)^{+1}/(TiO_2)^0$ interface results in polar catastrophe, and the charged $(LaO)^{+1}\ldots(AlO_2)^{-1}$ layers in the LAO film produce a built-in electric field of ~0.24 V/Å.[17] The corresponding electrostatic potential increases with increasing LAO thickness, and 2DEG appears at ~16 Å when the potential overcomes the energy discrepancy of 3.3 eV between the LAO valence band maximum and the STO conduction band minimum, resulting in a charge transfer from the LAO surface layer to the interface.[17] This scenario is consistent with the experiments in which an electric field originating from an external gating voltage can also induce the insulator-metal transition at LAO/STO interfaces.[11, 16, 18] In a later hard X-ray photoemission spectroscopy experiment, a discrepancy in the built-in fields between insulating and metallic

interfaces was indeed observed.[19] High-energy optical conductivity revealed an ~0.5e^- charge transfer from LAO into the interface.[20]

Based on the interfacial polar catastrophe, a recent work from Yang's group provided a group of combinatorial material descriptors with STO as the substrate and predicted 42 polar perovskite oxides that could form 2DEG at the interfaces.[21] However, far less conductive 2DEG systems have been experimentally discovered so far, indicating that other material parameters, including defect characteristics, must play a role. In fact, recent advances in oxide interfaces suggest that polar catastrophe alone is not sufficient to reconcile all experimental observations. The observation of a built-in field even in the conducting LAO/STO interface is inconsistent with the model in which the built-in field should be canceled after the charge transfer.[19, 22] Moreover, Segal *et al*. performed X-ray photoemission studies of the metal-insulator transition in LAO/STO and did not find the built-in field in the LAO or any dependence on substrate termination.[23] Several models involving various types of defects originating from polar catastrophe were developed, such as oxygen vacancies at the $LaAlO_3$ surface[24-26] and lattice distortions.[26-31] In addition to the polar catastrophe-related scenario, several extrinsic defects can also result in a metallic interface. In particular, conducting interfaces fabricated at very low oxygen pressures without post synthesis oxygen annealing are known to contain electron-donor oxygen vacancies at the interface.[3, 32-37] The redox reactions on the surface of $SrTiO_3$ substrates induced metallic interface between amorphous $LaAlO_3$, Al_2O_3, and yttria-stabilized zirconia films on $SrTiO_3$.[38, 39] Moreover, most $A^{3+}B^{3+}O_3$ oxides contain rare-earth elements, which promote the possible existence of donor defects by cation intermixing, leading to the formation of a metallic $La_{1-x}Sr_xTiO_3$ layer at the interface.[40-42]

Despite the ambiguous origin of 2DEG at the oxide interface, polar catastrophe is believed to be the most basic principle for designing new 2DEG systems.[13-15] One intriguing discovery in oxide interface research is that the polar catastrophe model can predict the formation of interfacial 2DEG in not only the LAO/STO case but also other systems, such as $LaTiO_3$/STO,[43, 44] $NdAlO_3$/STO,[45] and $LaGaO_3$/STO.[46] The polar catastrophe scenario also succeeds in designing a two-dimensional hole gas in $SrTiO_3/LaAlO_3/SrTiO_3$ heterostructures.[12] Thus, it is natural to explore novel 2DEG systems in materials with nonneutral layers to induce polar catastrophe at the interface through symmetry breaking. New 2DEG systems with other crystal structures have attracted considerable interest with the aim of unveiling the general design principle and developing applications. For example, a room-temperature, fully spin-polarized 2DEG has been forecasted for spin-field effect transistors based on spinel $CoFe_2O_4$ and $MgAl_2O_4$.[47] Nevertheless, only a few perovskite/perovskite heterostructures with the $A^{3+}B^{3+}O_3$ nonneutral formula have been reported to exhibit 2DEG to date.

Here, we report a new 2DEG system related to polar catastrophe in spinel/perovskite heterostructures. Spinel minerals with the general formulation of $A^{2+}B_2^{3+}O_4^{2-}$ possess alternative polar planes of A^{2+} and $(B_2O_4)^{2-}$ along the <001> direction, as shown in Figure 1a. Symmetry-breaking-induced polar catastrophe could be expected at the spinel/perovskite interface.[13, 48] The prototypical spinel mineral $MgAl_2O_4$ (MAO), after which this class of minerals is named, was selected to form the heterostructure with STO. MAO is a band insulator with an indirect band gap of 7.8 eV.[49] It has a face-centered cubic (FCC) Bravais lattice with space group $Fd\bar{3}m$. The oxygen atoms are arranged in a cubic close-packed lattice, and the cations Mg and Al occupy 1/8 of tetrahedral and 1/2 of octahedral sites within the oxygen sublattice, respectively.[50, 51] The lattice parameter of MAO is 8.083 Å, almost twice the lattice parameter of STO (3.905 Å),[50]

which leads to a lattice mismatch of 3.3% in MAO/STO, close to the case of LAO/STO (3.0%). The excellent match of oxygen sublattices and lattice constants between STO and MAO ensures the epitaxial growth of MAO on the STO substrate. As sketched in the ideal interface structure (Figure 1b), the stacking sequence at the interface of MAO/STO is $(Al_2O_4)^{2-}$-Mg^{2+}/$(TiO_2)^0$-$(SrO)^0$, suggesting the existence of polar catastrophe (Figure 1c). Moreover, there is no transition metal or rare-earth element in MAO, which prevents the electron donor in STO from involvement in cation intermixing. In an earlier report, Chen *et al.* observed a high-mobility 2DEG at the heterointerface between $SrTiO_3$ and spinel γ-Al_2O_3 (GAO) epitaxial film.[34] They found that the interface-stabilized oxygen vacancies induced by the oxygen-poor condition without annealing are responsible for the 2DEG. A detailed study of the band alignment in GAO/STO heterostructures by using hard x-ray photo-electron spectroscopy revealed band bending in the STO substrate and no signs for potential gradient in GAO.[52] Furthermore, theoretical calculations suggest that the lattice mismatch and intrinsic Al cation vacancies result in the interfacial reconstruction and lead to the insulator-metal transition.[53]

In this work, we report the 2DEG at the interface of spinel MAO and perovskite STO with a threshold thickness of 32.3 Å (4 unit cells) after *in situ* annealing at 1 atmosphere O_2. Combining high-angle annular dark field scanning transmission electron microscopy (HAADF-STEM) and first-principles calculations, a Ti-Al-O layer with a thickness of ~4 Å at the MAO/STO interface formed spontaneously due to the polar catastrophe, which cancels the build-in polar field in MAO and eventually induces conductivity at the MAO/STO interface. Our results on the MAO/STO interface open a new door for defect engineering of 2DEG at oxide interfaces.

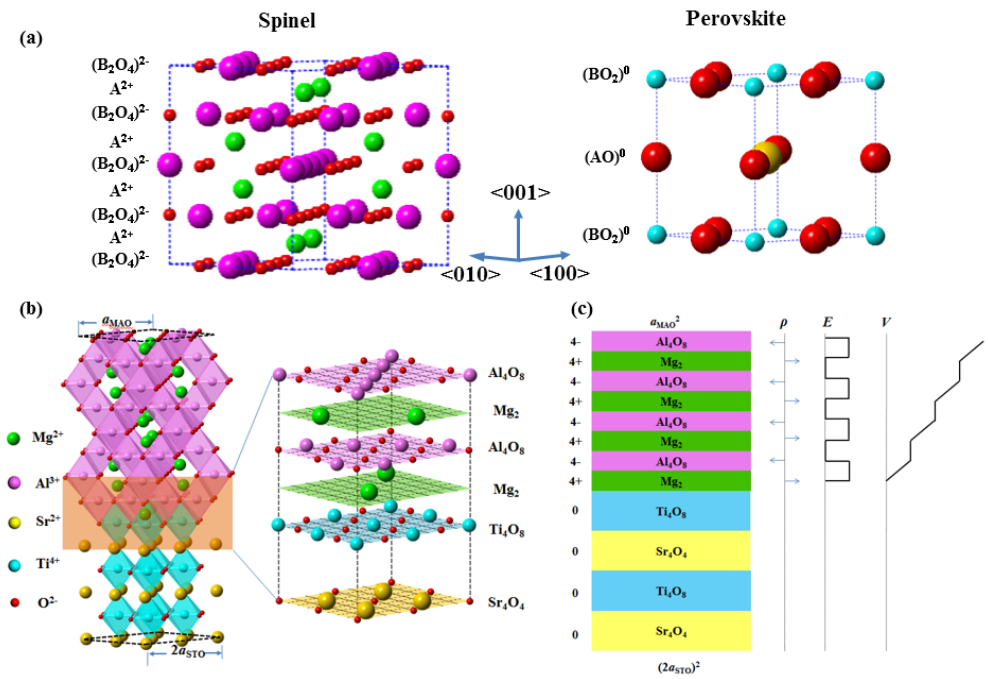

Figure 1. Polar catastrophe at the spinel/perovskite interface. (a) Crystal structure of a general spinel AB_2O_4 and a perovskite ABO_3. Spinel is composed of charged layers A^+ and $(B_2O_4)^-$, whereas the layers in perovskite are either charged or neutral. (b) Sketch of the spinel/perovskite heterojunction of $MgAl_2O_4/SrTiO_3$ (MAO/STO). Also shown is the ideal atomic distribution at the MAO/STO interface. Because of the good matching of the oxygen sublattices between the Ti_4O_8 layer in STO and the Al_4O_8 layer in MAO, the Mg_2 layer is supposed to be the first layer of MAO near the interface. (c) Schematic illustration of the polar catastrophe at the MAO/STO interface.

2. EXPERIMENTAL SECTION

$MgAl_2O_4/SrTiO_3$ heterostructures were fabricated at 800 °C by pulsed laser deposition on TiO_2 terminated STO substrate. During deposition, the laser influence was fixed at ~ 1 J/cm^2 and the oxygen pressure is 1×10^{-5} Torr. The thickness of MAO film was monitored by RHEED

oscillation. To remove oxygen vacancy, the temperature was decreased to 600 ºC, and the samples were annealed at 1 atmosphere O_2 pressure for 1 hour, then the chamber was slowly cooled down to room temperature. As a reference, oxygen-deficient STO was prepared after annealing at 800 °C and 1×10^{-5} Torr oxygen pressure for 1 hour, and then cooling down to room temperature with the same oxygen pressure. Charge transport properties of the MAO/STO sample were measured using the van der Pauw four-point method in a Physical Properties Measurement System (Quantum Design). Ti/Au was used as the contacts by sputtering.

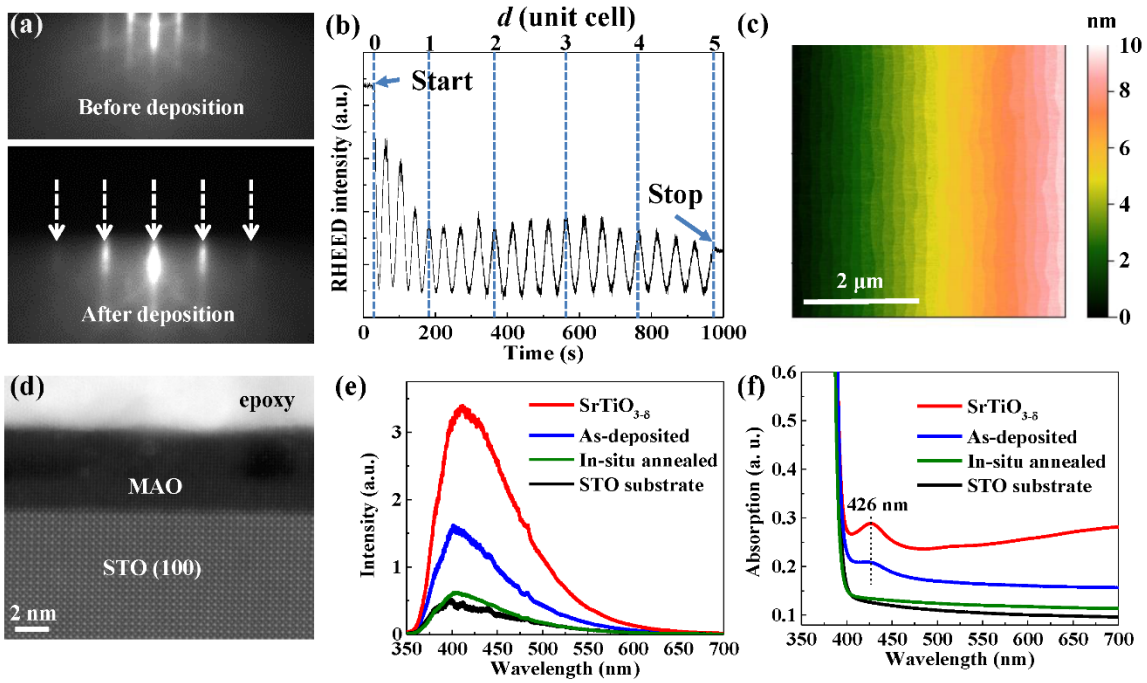

Figure 2. Layer-by-layer epitaxial growth of MAO on TiO_2 terminated STO. (a) RHEED patterns before and after the deposition of 5 unit cell MAO film. (b) Oscillations in RHEED intensity during growth suggest a layer-by-layer growth mode. (c) AFM image of the same film, confirming the layer-by-layer growth. (d) HAADF image of a 6 unit cell MAO on STO. (e) PL spectra and (f) absorption of 10 unit cell MAO/STO with and without in situ annealing at 600 °C

and 1 atm O_2 pressure. The as-received STO substrate and vacuum-annealed STO were also measured as references.

First-principles calculations were performed using density functional theory (DFT), as implemented in the Vienna Ab-initio Simulation Package (VASP).[54, 55] The Projector Augmented Wave (PAW) potentials were used for describing electron-ion interactions[56] and the Generalized-Gradient Approximation (GGA) was applied for the exchange-correlation functional.[57] The cutoff energy for the plane wave expansion was set to 450 eV. Gamma-centered *k*-point grids for Brillouin zone sampling were set to $3\times3\times1$ for ionic relaxation and $6\times6\times1$ for static calculations, respectively. To reproduce the experimental epitaxial growth of the film, all the atomic positions and the lattice parameters along the z-axis (i.e., perpendicular to the interfacial plane) of the heterostructure model were fully relaxed by minimizing the forces up to 0.03 eV/Å. The cell parameter along the interfacial plane was fixed as the 7.87Å, *i.e.*, twice of the bulk STO equilibrium lattice parameter ($a = 3.935$ Å). The convergence tolerance of the total energy was set to 10^{-5} eV.

3. RESULTS AND DISCUSSION

Layer-by-layer growth of $MgAl_2O_4$ on $SrTiO_3$. MAO films were deposited on TiO_2-terminated STO substrate by pulsed laser deposition at 800 °C under 1×10^{-5} Torr oxygen pressure followed by one hour of annealing at 600 °C and 1 atmosphere O_2 pressure to remove oxygen vacancies. Before deposition, the reflection high-energy electron diffraction (RHEED) pattern showed a clear (100) symmetry of the STO substrate (see Figure 2a). Due to the difference in lattice symmetry between the MAO film and the STO substrate, the distances of the RHEED patterns were doubled after the deposition of the MAO layer. The oscillations in

RHEED intensity during growth suggest a layer-by-layer growth mode, as shown in Figure 2b. Each oscillation period corresponds to the minimum unit of the chemical composition needed to ensure charge neutrality. Thus, 4 oscillations indicate the growth of 1 unit cell MAO layer. The step-like pattern in the atomic force microscopy (AFM) image of Figure 2(c) confirms the layer-by-layer growth of the MAO film. The height of the step is approximately 3.9 Å, which represents the step of the TiO_2-terminated STO substrate. In Figure 2(d), the cross-section HAADF image of the MAO/STO heterojunction suggests good epitaxial growth of MAO on the STO and the sharp interface. As the contrast in this technique is related to the atomic number Z, the MAO layer appears darker than the STO substrate because of the lower average Z numbers (Mg-12, Al-13, Ti-22, and Sr-38).

Ti-Al antisite defects at the MAO/STO interface. Figure 3a shows the HAADF-STEM blowup image at the MAO/STO interface. Based on the contrast of ions with different Z values, the ion distribution can be illustrated as reported in the literature.[58] The interface layer cannot be labeled either TiO_2 or AlO_2. In fact, the HAADF signal profile along the <001> direction in Figure 3c indicates that Ti diffused into the adjacent MAO layer in proximity to the interface. A clear stack sequence (-Sr-O-)/(-Ti-Al-O-)/(-Ti-Al-O-)/(-Al-O-) can be observed from the layer-resolved HAADF signal profile, as shown in Figure 3b, indicating the formation of two Ti-Al-O atomic layers at the MAO/STO interface. There are two interesting properties of the interfacial Ti-Al antisite defects in the MAO/STO heterostructure. First, the abrupt drop of the Ti signal in Figure 3c suggests that the Ti-Al antisite defects are strongly confined at the interface. The thickness of the interfacial Ti-Al-O layer estimated from Figure 3c is approximately 4 Å, indicating an important role in the interfacial electron and/or orbital reconstruction at MAO/STO. Second, at the interfacial layers, the Ti ions do not randomly occupy the positions of

Al ions but follow the crystal structure of STO, as shown in Figure 3b. Ti ions retain the B site of perovskite ABO_3 in the Ti-Al-O layer at the $SrTiO_3$ side and represent the A site of Sr ions in the Ti-Al-O layer at the MAO side. This distribution in MAO/STO suggests the prominent role of the oxygen sublattice on the interface structure. Element intermixing within several monolayers at the interface is ubiquitous in both metallic and insulating LAO/STO samples.[12, 13, 27] STEM-EELS mapping of LAO/STO shows that Ti diffuses across the interface to $LaAlO_3$ layers for approximately 2 unit cells, where the Al fraction gradually decreases from bulk to the interface,[27] indicating a coexistence of Ti ions and Al ions at the interface, which is consistent with our HAADF-STEM results of a Ti-Al-O monolayer at the MAO/STO interface.

To further investigate the element intermixing at the MAO/STO interface, Rutherford backscattering spectrometry (RBS) was performed on the sample of 10-unit-cell MAO on STO substrate, as shown in Figure S1 of supplementary material. In RBS, the incident He^+ ions are scattered by nuclei of the elements in the material. An energy spectrum of the backscattered He^+ ions yields information about the elements at different depth, and can be used to study the buried interfaces and diffusion profiles.[59] The double peaks of Al in the RBS suggest the distribution of Al is inhomogeneous in different layers. The fitting of the spectrum indicates an interfacial Al-Ti-O mixing layer, which supports our claim of an interfacial Ti-Al-O layer. However, due to the small atomic number the signal of Mg in the RBS is too weak to extract its distribution in MAO/STO.

Oxygen vacancy defects. Photoluminescence (PL) and absorption spectra were collected to check the influence of oxygen pressure during growth on the oxygen deficiency of the samples. The STO substrate and vacuum-annealed STO were also measured for reference. As shown in Figure 2(e) and (f), the sample without annealing shows a stronger PL, which suggests the

existence of a large amount of oxygen vacancies.[60, 61] After annealing, the PL intensity decreases to a level close to that of the insulating STO substrates. The absorption edges of all the samples are located at 380 nm, which corresponds to the band gap of STO (3.2 eV). The annealed STO substrate and the as-deposited MAO/STO heterostructure show another absorption peak at approximately 426 nm, suggesting the existence of donor levels associated with oxygen vacancies below the bottom of the conduction band of STO.[62] After annealing, the absorption peak from the oxygen vacancy states disappears, and the absorption across the entire measured wavelength region decreases to a value near that of the insulating STO substrate. The PL and absorption spectra suggest that the in situ annealing process sufficiently reduces the oxygen vacancy defects in the MAO/STO heterointerface.[63] It should be noted that a small amount of oxygen vacancies may still exist at the interface, which has been suggested to be responsible for the interface conductivity in some titanium oxide based heterostructures. [3]

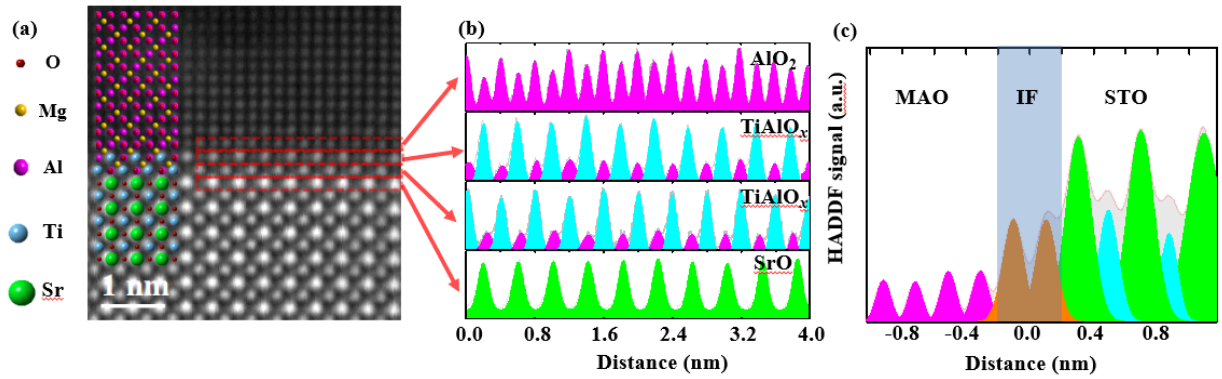

Figure 3. Ti-Al antisite defects at the MAO/STO interface. (a) HAADF-STEM image and the corresponding schematic structures of MAO and STO. Sr, Ti, and Al ions can be clearly distinguished due to their different Z values. (b) Layer-resolved HAADF signal profiles from

areas outlined in (a) along the direction parallel to the interface for four atomic layers around the interface. Green, cyan, and magenta peaks denote Sr, Ti, and Al atoms, respectively. The coexistence of Ti and Al implies the formation of interfacial Ti-Al antisite defects. (c) Signal profile extracted from the HAADF image along the direction perpendicular to the interface suggests that the interfacial Ti-Al antisite defects are confined within a thickness of approximately 4 Å. IF is the abbreviation of interface.

Charge transport of the 2DEG at MAO/STO interface. As shown in Figure 4a, although both MAO and STO are band-insulators, the temperature-dependent resistances of MAO/STO samples present metallic behavior when the MAO layer exceeds 4 unit cell (32.3 Å). The thickness dependencies of conductivity and charge density at room temperature show a threshold at 4 unit cell (Figure 4b), and the resistances of samples with a thinner MAO layer are outside the measurement limit (10^9 Ohm). Although the 2DEG reported in LAO/STO interfaces also has a threshold of approximately 4 unit cell,[16] the lattice parameter of MAO, a = 8.083 Å, is twice as large as that of LAO (~3.8 Å). Hall measurement shows that the main type of charge is electron with a charge density of 5.2×10^{13} cm^{-2} and a mobility of 304 cm^2/Vs for the 10 unit cell MAO/STO at 2 K, which is similar to the values reported for LAO/STO interfaces.[15, 16, 64] The temperature dependencies of resistance for all the samples show a low-temperature upturn, which is commonly observed in systems with symmetry breaking. The resistance upturn could be attributed to the weak localization (WL) as a result of the interface disorders or to the Kondo effect with a magnetic origin. In the MAO/STO system, a positive magnetoresistance was observed, implying that the charge transport is not likely to be dominated by the Kondo effect, which usually results in a negative magnetoresistance due to the suppression of spin-flip scattering under a magnetic field.[65]

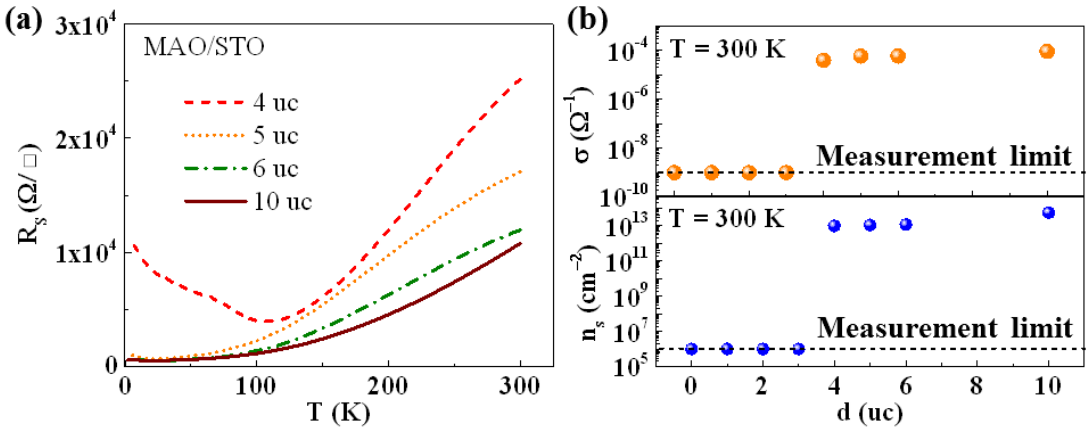

Figure 4. Thickness dependence of 2DEG at MAO/STO heterostructure. (a) Sheet resistance of the MAO/STO samples with different MAO layer thicknesses. (b) Thickness dependencies of the conductivity and charge density at room temperature for MAO/STO. The resistances of the samples with a thickness less than 4 unit cell are outside the measurement limit. The charge density of the metallic interfaces at room temperature is at the level of 10^{-13} cm^{-2}.

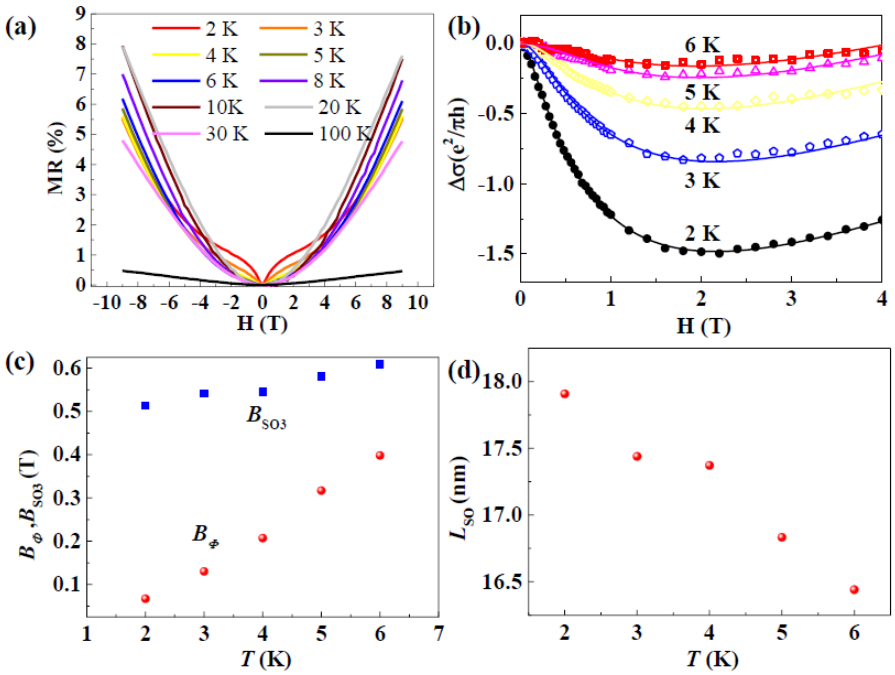

Figure 5. Weak antilocalization induced by the Rashba spin-orbit interaction. (a) Magnetoresistance of the 10 unit cell MAO on STO. The applied magnetic field is perpendicular to the film plane. (b) Experimental $\Delta\sigma$ (symbols) and theoretical fits (lines) to the k-cubic ILP model. (c) Parameters used for the k-cubic ILP fitting (B_{SO1}=0). (d) Temperature dependence of the spin precession length.

Arising from the structural inversion symmetry breaking, the Rashba spin-orbit interaction can be substantial and plays a critical role in the charge transport for 2DEG systems.[66-68] According to the weak antilocalization (WAL) theory, the destructive interference effect of coherently back-scattered electrons enhances the conductivity of the system. The applied out-of-plane magnetic field suppresses the conduction enhancement and hence results in a sharp increase in resistance at low fields. In Figure 5a, the magnetoresistance (MR) of the MAO/STO interface shows a sharp cusp at a magnetic field of 0 T for temperatures below 6 K, which is a typical WAL feature in a 2DEG system.[69] The conductivity difference $\Delta\sigma$, which presents a WAL correction to the conductivity by subtracting the B^2 Lorentz background, can be fitted by the k^3 spin splitting model from the Iordanskii, Lyanda-Geller, and Pikus (ILP) theory, as shown in Figure 5b.[69] Figure 5c shows the fitting parameters characterizing the magnetic fields for the phase coherence B_Φ and the spin-orbit coupling B_{SO3}. The spin precession length L_{SO} calculated from the fitting is approximately 18 nm at 2 K (Figure 5d), which is smaller than the value of 60 nm reported on electrically gated $SrTiO_3$.[69, 70] The shorter L_{SO} probably reflects that the atomic spin-orbit coupling is stronger in MAO/STO than in the electrically gated $SrTiO_3$.

Temperature-dependent resistance and the magnetoresistance data reveal a competition between WL and WAL effects in the MAO/STO. The resistance upturn appears at around 21 K, and the negative magnetoconductivity cannot be clearly distinguished above 6 K, which imply a

transition from WL to WAL as the dominant effect with decreasing temperature. We also could not exclude the scenario that the electron-electron interaction leads to the resistance upturn, which has been reported in topological insulators.[71] The electron-electron interaction may dominate the temperature dependent behavior, but not respond significantly to the external magnetic field.

Origin of the 2DEG in MAO/STO. We first evaluated the 2DEG in this new type of interface using the polar catastrophe model without defects. In the polar catastrophe model, the critical thickness of the interfacial 2DEG can be calculated from equation (1) as follows:

$$L = \Delta\Phi\epsilon_0\varepsilon_r/eP_0 \quad (1)$$

where $\Delta\Phi$ is the energy difference between the film valence band maximum and the STO conduction band minimum, and ε_r and P_0 are the relative permittivity and formal polarization of the film, respectively.[72] For the prototype LAO/STO model, the critical thickness L of LAO to form interfacial 2DEG is approximately 13.5 Å with the parameters ε_r = 24.5, $\Delta\Phi$ ~3.3 eV, P_0= 0.529 Cm^{-2}, which is consistent with the experimental value of 4 unit cell.[25, 72] For the 2DEG at the MAO/STO interface, by using the physical parameters ε_r = 7.89,[47] $\Delta\Phi$ ~3.8 eV (see Figure S2 in the Supplementary Information), and $P_{MAO} = 4e/2S_{MAO}$, the critical thickness is estimated to be 5.0 Å, which means the 2DEG should arise in 1 unit cell MAO (8.08 Å) films and is inconsistent with the experimental value of 4 unit cell.

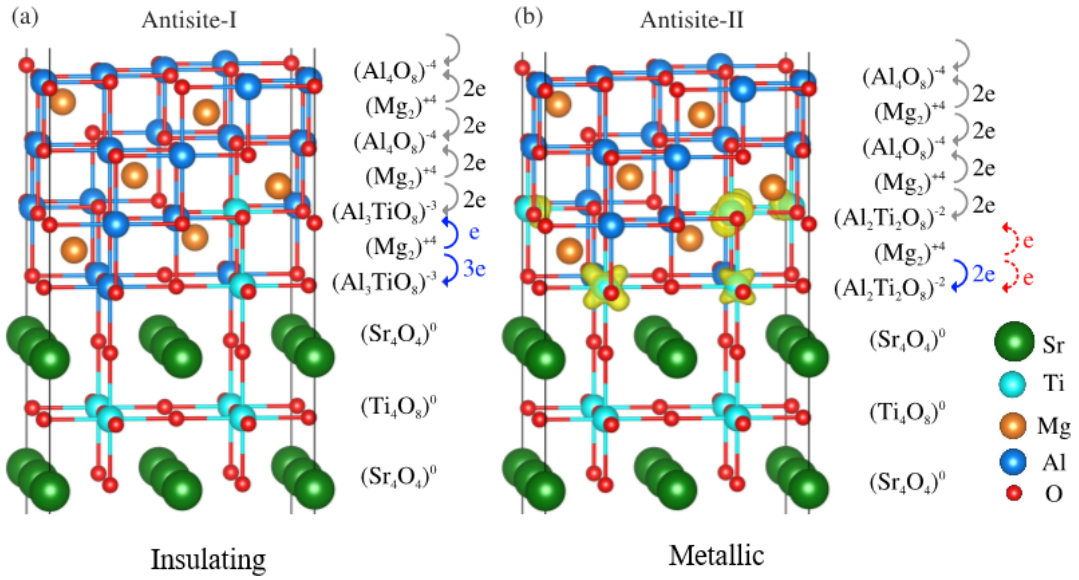

Figure 6. Antisite defect models to explain the 2DEG at MAO/STO interfaces. Heterostructure models of (a) Antisite-I and (b) Antisite-II along with the charge density projected on the bands forming interfacial conductivity and the charge transfer mechanism. The yellow color around the Ti ion in (b) indicates the conducting 3*d* orbital. Considering the polar catastrophe at the MAO/STO interface with antisite defects, Antisite-I is insulating, and Antisite-II is metallic.

To understand the origin of 2DEG at the MAO/STO interface and the large discrepancy between the estimated and experimental critical thickness of the insulator-to-metal transition, we studied the electronic structures and energetic stability of the MAO/STO system using first-principles density functional theory (DFT) calculations. We built MAO/STO heterostructure-based slab models with different MAO layer thicknesses and calculated their electronic structures. The conventional unit cell of MAO contains four alternating layers of $[Mg_2]^{4+}$ and $[Al_4O_8]^{4-}$, as shown in Figure 1. To be clear, one alternating $[Mg_2]^{4+}$ and $[Al_4O_8]^{4-}$ layer is defined

as one monolayer (ML); thus, one MAO unit cell contains 4 MLs. The layer-resolved density of states (DOS) of the MAO/STO model with 4ML MAO is shown in Figure S4 of the Supplementary Information. Driven by the polar catastrophe at the $(Mg_2)^{4+}/(Ti_4O_8)^0$ interface, Ti 3*d* states near the interface cross the Fermi level and become occupied, forming *n*-type conductivity at the interface, similar to the LAO/STO case. The total DOS for the MAO/STO slab shows that the MAO/STO heterostructure has an insulator-to-metal transition when the MAO thickness increases up to 4ML, *i.e.*, one MAO unit cell (8.08 Å); see Figure S5 in the Supplementary Information. The large discrepancy between the calculated critical thickness (8.08 Å) and the experimental value (32.3 Å) suggests that the 2DEG in MAO/STO is not caused solely by the polar-catastrophe-induced charge transfer.

We built two antisite defect models for the MAO/STO interface and studied its thermodynamic stability and electronic properties. Our structural models are based on three experimental evidences: i) our HAADF measurement shows the existence of Ti-Al antisite defects, which is similar to the $LaAlO_3/SrTiO_3$ interface with extensive Sr-La and Ti-Al antisite defects.[43] ii) growth-induced non-stoichiometry, such as an Al-excess film, in $LaAlO_3/SrTiO_3$ [75] may also exist in MAO/STO, which makes the antisite model reasonable, and iii) the experimentally observed critical thickness of the MAO film to form interfacial conductivity is 32.3 Å, which is much larger than the calculated value of 8.08 Å from the defect-free model. Herein, we modeled two types of antisite defect models: i) Antisite-I with one Ti-Al antisite set plus two substitutional Al to Ti atoms at the interfacial $(Ti_4O_8)^0$ layer, which forms the symmetrical $(Al_3TiO_8)^{-3}$-$(Mg_2)^{+4}$-$(Al_3TiO_8)^{-3}$ structure (see Figure 6a), and ii) Antisite-II with two Ti-Al antisite sets at the interface, which forms symmetrical $(Al_2Ti_2O_8)^{-2}$-$(Mg_2)^{+4}$-$(Al_2Ti_2O_8)^{-2}$ structure (see Figure 6b). For Antisite-I, the built-in field is canceled by the formation of an

interface $(Al_3TiO_8)^{-3}$ layer, and the potential remains finite. The interfacial $(Mg_2)^{+4}$ layer donates four electrons to the two adjacent $(Al_3TiO_8)^{-3}$ layers. One electron goes to the upper $(Al_3TiO_8)^{-3}$ layer, and the other three go to the lower $(Al_3TiO_8)^{-3}$ layer, leading to a charge balance. As a result, the interface at Antisite-I is insulating. In Antisite-II, to maintain the charge balance between the interfacial $(Mg_2)^{+4}$ layer and its adjacent two $(Al_2Ti_2O_8)^{-2}$ layers, the interfacial $(Mg_2)^{+4}$ layer needs only to donate two electrons to the lower $(Al_2Ti_2O_8)^{-2}$ layer since the upper $(Al_3TiO_8)^{-2}$ layer can accept two electrons from the upper $(Mg_2)^{+4}$ layer. As a result, the interfacial $(Mg_2)^{+4}$ layer donates two remaining electrons that are captured by Ti 3*d* orbitals in the adjacent two $(Al_3TiO_8)^{-2}$ layers, forming a conducting interface (see Figure 6b). Thus, both the insulating and metallic interface can rise in the Ti-Al antisite defects model, which may explain the thickness-dependent 2DEG in MAO/STO.

To evaluate the relative stability of the two antisite models, we calculated their defect formation energies, as shown in Figure 7a. The details of the calculations can be found in the Supplementary Information. The negative formation energy of the Antisite-I model indicates the spontaneous formation of Antisite-I, while Antisite-II is energetically unfavorable. This suggests that the MAO/STO interfaces with antisite Ti-Al defects tend to be insulating rather than metallic, which is consistent with the insulating MAO/STO interface below the critical thickness, but the antisite model alone cannot explain the metallicity in thicker films.

It is worth pointing out that recent theoretical studies have shown that oxygen vacancies also exist on the surface of the $LaAlO_3$ film due to the intrinsic charge imbalance[25, 74, 75]. Yu *et al.* found that the oxygen vacancies at the surface are more stable than those at the interface, and they even exist after exposure to air or post-annealing in an O-rich environment in LAO/STO.[25] Based on these considerations, we built the MAO/STO heterostructure with both interfacial Ti-

Al antisites (Antisite-I and Antisite-II) and surface oxygen vacancies and studied their energetic stability. For the convenience of discussion, they are named Antisite-I-Vo and Antisite-II-Vo, respectively, both with one oxygen vacancy on the $(Al_4O_8)^{4-}$ surface layer.

To evaluate the formation possibility of Antisite-II-Vo, we calculated its formation energy as a function of the oxygen chemical potential at various MAO thicknesses (Figure 7b). The details of the calculation of formation energy are shown in the Supplementary Information. Our calculations show that the formation energy decreases with increasing MAO thickness, which indicates that the oxygen vacancy becomes more energetically favorable with thicker MAO film. As the oxygen chemical potential $\Delta\mu_O$ under the deposition condition (T = 800 °C and P = 1×10^{-5} Torr) is -6.95 eV (see details in the Supplementary Information), the formation energy becomes negative for a 3 unit cell MAO film (~2.42 nm), as shown in Figure 7b, indicating the spontaneous formation of Antisite-II-Vo. In other words, the surface oxygen vacancies promote the formation of metallic Antisite-II layer.. This thickness threshold is close to the experimentally observed critical thickness of 4 unit cells of MAO (~3.23 nm). We attribute the small discrepancy in the critical thickness to the following two factors: (1) the coexistence of the insulating Antisite-I with a similar formation enthalpy ΔH. The conducting channel appears in the insulating background of Antisite-I when more Antisite-II defects arise in thicker MAO films. (2) the removal of oxygen vacancies during in situ annealing. In Figure S4, we plot the formation energy of Antisite-II-Vo as function of the MAO thickness under annealing conditions. We found that the spontaneous formation of surface oxygen vacancy happens when the MAO thickness is larger than 4.7 nm (~6 unit cells of MAO).

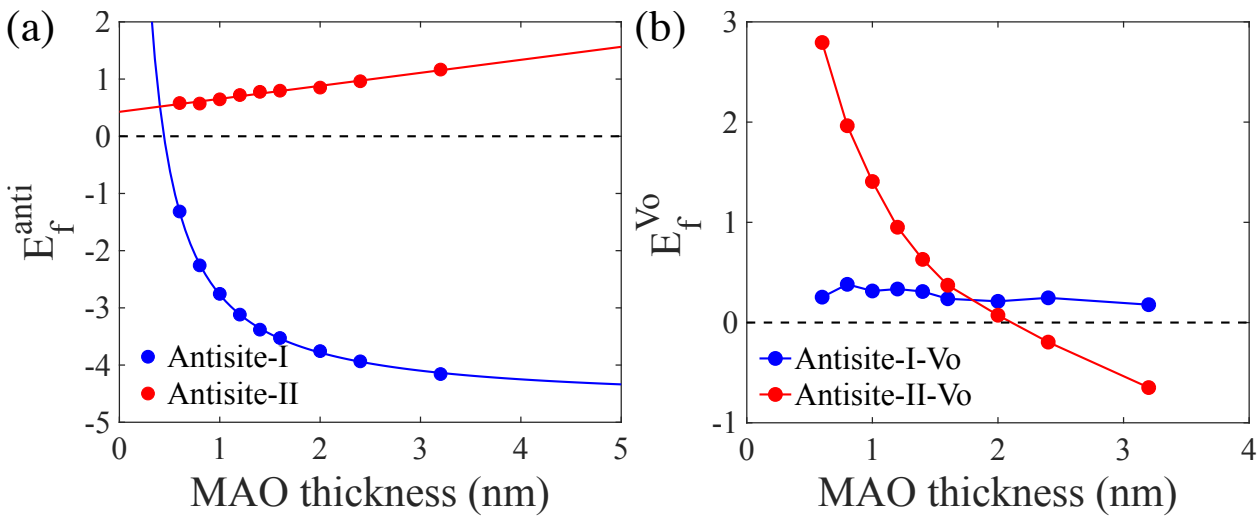

Figure 7. Thickness-dependent formation of antisite defects and surface oxygen vacancies. (a) Calculated defect formation energy (E_f^{anti}) for Antisite-I and Antisite-II as a function of the $MgAl_2O_4$ film thickness. (b) Calculated formation energy of Antisite-II-Vo and Antisite-II-Vo as a function of MAO thickness under the experimental deposition conditions.

Discussions. Our discovery of the 2DEG at the MAO/STO interface provides a platform for both the exciting physics and oxide electronic applications of interfacial 2DEG. The MAO/STO interface is an excellent reference system for comparing with the LAO/STO counterpart to unveil the physics of 2DEG at the oxide interface. Due to the ubiquitous nature of interfacial defects, it is quite a challenge to identify the exact role of defects in the 2DEG. For example, all the examples of 2DEG in perovskite/perovskite heterostructures contain rare-earth elements, which may induce the metallic interface by an unexpected cation mixture, such as $La_xSr_{1-x}TiO_3$ in LAO/STO.[59] Although several theoretical works have shown that such a cation mixture at the interface leads to an insulator, there is no direct experimental evidence to demonstrate that 2DEG can exist without rare-earth element intermixture in a perovskite/perovskite system.[25] In fact, several experiments have observed the intermixture of La at the interfaces of LAO/STO and

attribute the 2DEG to the rare-earth element doping.[32, 59] In our spinel/perovskite system, there are no rare-earth elements. Thus, the 2DEG at MAO/STO with similar electrical properties to LAO/STO directly excludes the rare-earth doping mechanism for 2DEG at the oxide interface. Moreover, the discrepancy between the observed critical thickness of 4 unit cell and the calculated value of 1 unit cell using a polar-catastrophe-induced charge transfer model suggests that the polar catastrophe alone is not enough for the emergence of 2DEG, and spontaneous interfacial defects in MAO/STO must be considered.

Besides the antisite defects model in the present work, two other scenarios may contribute to the interface conductivity in MAO/STO. First, oxygen vacancies have been observed in various oxide heterostructures and supposed to result in the interfacial conductivities in some titanium oxide based 2DEG systems. Although the annealing process conducted *in situ* at 600 °C and 1 atmosphere O_2 could reduce the oxygen vacancy level in the bulk, a small amount of oxygen vacancy may still exist at the interface of MAO/STO. Both the earlier theoretical work[25] and our calculations suggest that several kinds of oxygen vacancy can be robust against annealing but they are not expected to dictate the transport behavior. Second, lattice distortion has been reported in LAO/STO and results in the ferroelectric-like polarizations across the interface.[27] Recent theoretical calculations on GAO/STO also suggest that the lattice mismatch at interface could induce lattice distortion and spontaneous polarization in the GAO part. [53] The lattice mismatch in MAO/STO is close to that in LAO/STO and GAO/STO, and thus lattice distortion at the interface may also exist and warrants future investigation.

The 2DEG at the MAO/STO interface also introduces new opportunities for oxide electronic applications. First, without expensive rare-earth elements, MAO/STO could be a less expensive alternative to LAO/STO for various applications, such as memory devices based on resistive

switching.[24] Second, MAO has been commonly adopted as the buffer layer for ferrimagnetic spinels deposited on perovskite STO.[76] Here, we show that this bottom MAO/STO interface is conductive and thus could be used as a transparent electrode for constructing multilayer magnetic devices. Finally, the reports of 2DEG at the spinel/perovskite interface could attract new efforts to design novel spintronic devices based on perovskite/spinel heterostructures. Recently, magnetic tunnel junctions with MAO barriers were reported to exhibit giant tunnel magnetoresistance for the application of high-performance spintronic devices.[49, 50] Our results highlight the prominent role of symmetric breaking-induced polar catastrophe and Rashba spin-orbit interactions in the charge transport properties at the interface. Furthermore, there is a large group of spinels with various properties and broad applications, such as antiferromagnetic insulators, ferromagnetic metal/insulators, and superconductors. In particular, half-metallic ferromagnetic Fe_3O_4 has been intensively investigated to integrate it into spintronic devices. The insulating nature of ferrimagnetic $NiFe_2O_4$ or $CoFe_2O_4$ spinels makes these materials suitable for tunnel barriers in room-temperature spin filters or magnetoelectric multiferroic composites.[77]

4. CONCLUSIONS

In this work, spinel $MgAl_2O_4$ films were epitaxially grown on perovskite $SrTiO_3$ in the layer-by-layer mode followed by in situ annealing in an oxygen atmosphere. Charge transport measurements revealed a new 2DEG at the interface of MAO/STO with a thickness dependence different from the LAO/STO system. Interfacial Ti-Al-O layers were observed in the HAADF-STEM images. The first-principles calculations suggest that Ti-Al antisite defects form spontaneously due to the polar catastrophe at the interface and cancel the built-in polar field in MAO. The coexistence and competition of different types of Ti-Al antisite defects lead to the thickness dependence of the metallic interface. Our complementary experimental and calculation

results regarding the critical role of antisite defects at the MAO/LAO interface underscore the importance of defect engineering in addition to the polar catastrophe, which opens a new door for interface design with tailored properties.

ASSOCIATED CONTENT

Supporting Information

The following files are available free of charge. A band diagram of the metallic MAO/STO interface, calculated layer-resolved partial DOS for defect-free MAO/STO, calculated total DOS for MAO/STO HS-based slab various MAO thicknesses, formation energy of Antisite-II with surface oxygen vacancy.

AUTHOR INFORMATION

Corresponding Author

*Correspondence and requests for materials should be addressed to K. Y. (email：kesong@ucsd.edu) or T. W. (email: tom.wu@unsw.edu.au)

Notes

The authors declare no competing financial interest.

ACKNOWLEDGMENT

This work was supported by National Natural Science Foundation of China (Grant Nos. 51672279, 51727806, 11874361, and 11774354), Science Challenge Project (No. TZ2016001), and the CASHIPS Director's Fund (Grant No. YZJJ201705). K.Y acknowledges the support from the National Science Foundation under award number ACI-1550404. The computational

work used the Extreme Science and Engineering Discovery Environment (XSEDE), which is supported by National Science Foundation grant number ACI-1548562.

For Table of Contents Only

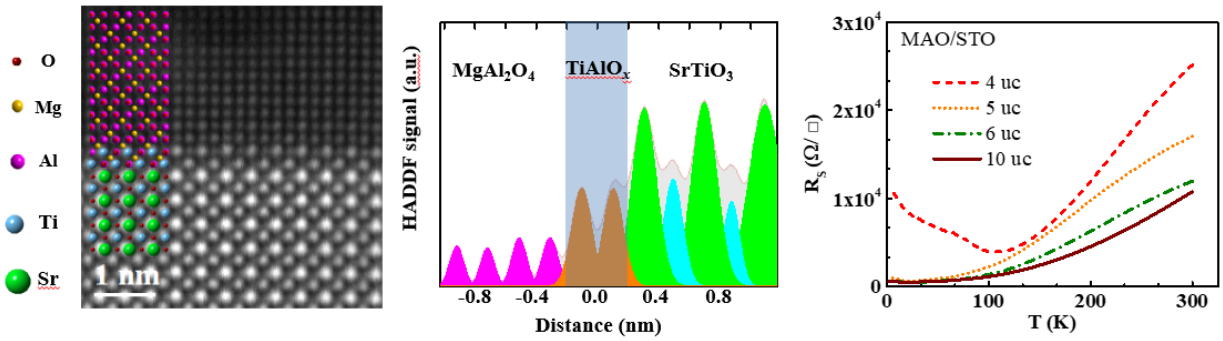

REFERENCES

(1) Hwang, H. Y.; Iwasa, Y.; Kawasaki, M.; Keimer, B.; Nagaosa, N.; Tokura, Y. Emergent Phenomena at Oxide Interfaces. *Nat. Mater.* **2012**, *11*, 103-113.
(2) Wang, B.; You, L.; Ren, P.; Yin, X.; Peng, Y.; Xia, B.; Wang, L.; Yu, X.; Mui Poh, S.; Yang, P.; Yuan, G.; Chen, L.; Rusydi, A.; Wang, J. Oxygen-Driven Anisotropic Transport in Ultra-Thin Manganite Films. *Nat. Commun.* **2013**, *4*, 2778.
(3) Rödel, T. C.; Fortuna, F.; Sengupta, S.; Frantzeskakis, E.; Fèvre, P. L.; Bertran, F.; Mercey, B.; Matzen, S.; Agnus, G.; Maroutian, T.; Lecoeur, P.; Santander-Syro, A. F. Universal Fabrication of 2d Electron Systems in Functional Oxides. *Adv. Mater.* **2016**, *28*, 1976-1980.
(4) Zhang, W.; Li, M.; Chen, A.; Li, L.; Zhu, Y.; Xia, Z.; Lu, P.; Boullay, P.; Wu, L.; Zhu, Y.; MacManus-Driscoll, J. L.; Jia, Q.; Zhou, H.; Narayan, J.; Zhang, X.; Wang, H. Two-Dimensional Layered Oxide Structures Tailored by Self-Assembled Layer Stacking Via Interfacial Strain. *ACS Appl. Mater. Inter.* **2016**, *8*, 16845-16851.
(5) Ohtomo, A.; Hwang, H. Y. A High-Mobility Electron Gas at the LaAlO3/SrTiO3 Heterointerface. *Nature* **2004**, *427*, 423-426.
(6) Park, J. W.; Bogorin, D. F.; Cen, C.; Felker, D. A.; Zhang, Y.; Nelson, C. T.; Bark, C. W.; Folkman, C. M.; Pan, X. Q.; Rzchowski, M. S.; Levy, J.; Eom, C. B. Creation of a Two-Dimensional Electron Gas at an Oxide Interface on Silicon. *Nat. Commun.* **2010**, *1*, 94.
(7) Chen, Y. Z.; Trier, F.; Wijnands, T.; Green, R. J.; Gauquelin, N.; Egoavil, R.; Christensen, D. V.; Koster, G.; Huijben, M.; Bovet, N.; Macke, S.; He, F.; Sutarto, R.; Andersen, N. H.; Sulpizio, J. A.; Honig, M.; Prawiroatmodjo, G. E. D. K.; Jespersen, T. S.; Linderoth, S.; Ilani, S.; Verbeeck, J.; Van Tendeloo, G.; Rijnders, G.; Sawatzky, G. A.; Pryds, N. Extreme Mobility Enhancement of Two-Dimensional Electron Gases at Oxide Interfaces by Charge-Transfer-Induced Modulation Doping. *Nat. Mater.* **2015**, *14*, 801-806.
(8) Lin, W.; Li, L.; Doğan, F.; Li, C.; Rotella, H.; Yu, X.; Zhang, B.; Li, Y.; Lew, W. S.; Wang, S.; Prellier, W.; Pennycook, S. J.; Chen, J.; Zhong, Z.; Manchon, A.; Wu, T. Interface-Based

Tuning of Rashba Spin-Orbit Interaction in Asymmetric Oxide Heterostructures with 3d Electrons. *Nat. Commun.* **2019**, *10*, 3052.
(9) Reyren, N.; Thiel, S.; Caviglia, A. D.; Kourkoutis, L. F.; Hammerl, G.; Richter, C.; Schneider, C. W.; Kopp, T.; Rüetschi, A.-S.; Jaccard, D.; Gabay, M.; Muller, D. A.; Triscone, J.-M.; Mannhart, J. Superconducting Interfaces between Insulating Oxides. *Science* **2007**, *317*, 1196-1199.
(10) Brinkman, A.; Huijben, M.; van Zalk, M.; Huijben, J.; Zeitler, U.; Maan, J. C.; van der Wiel, W. G.; Rijnders, G.; Blank, D. H. A.; Hilgenkamp, H. Magnetic Effects at the Interface between Non-Magnetic Oxides. *Nat. Mater.* **2007**, *6*, 493-496.
(11) Lin, W.-N.; Ding, J.-F.; Wu, S.-X.; Li, Y.-F.; Lourembam, J.; Shannigrahi, S.; Wang, S.-J.; Wu, T. Electrostatic Modulation of LaAlO3/SrTiO3 Interface Transport in an Electric Double-Layer Transistor. *Adv. Mater. Interfaces* **2013**, *1*, 1300001.
(12) Lee, H.; Campbell, N.; Lee, J.; Asel, T. J.; Paudel, T. R.; Zhou, H.; Lee, J. W.; Noesges, B.; Seo, J.; Park, B.; Brillson, L. J.; Oh, S. H.; Tsymbal, E. Y.; Rzchowski, M. S.; Eom, C. B. Direct Observation of a Two-Dimensional Hole Gas at Oxide Interfaces. *Nat. Mater.* **2018**, *17*, 231-236.
(13) Nakagawa, N.; Hwang, H. Y.; Muller, D. A. Why Some Interfaces Cannot Be Sharp. *Nat. Mater.* **2006**, *5*, 204-209.
(14) Caviglia, A. D.; Gariglio, S.; Cancellieri, C.; Sacépé, B.; Fête, A.; Reyren, N.; Gabay, M.; Morpurgo, A. F.; Triscone, J. M. Two-Dimensional Quantum Oscillations of the Conductance at LaAlO3/SrTiO3 Interfaces. *Phys. Rev. Lett.* **2010**, *105*, 236802.
(15) Bark, C. W.; Felker, D. A.; Wang, Y.; Zhang, Y.; Jang, H. W.; Folkman, C. M.; Park, J. W.; Baek, S. H.; Zhou, H.; Fong, D. D.; Pan, X. Q.; Tsymbal, E. Y.; Rzchowski, M. S.; Eom, C. B. Tailoring a Two-Dimensional Electron Gas at the LaAlO3/SrTiO3 (001) Interface by Epitaxial Strain. *Proc. Natl. Acad. Sci.* **2011**, *108*, 4720-4724.
(16) Thiel, S.; Hammerl, G.; Schmehl, A.; Schneider, C. W.; Mannhart, J. Tunable Quasi-Two-Dimensional Electron Gases in Oxide Heterostructures. *Science* **2006**, *313*, 1942-1945.
(17) Cancellieri, C.; Fontaine, D.; Gariglio, S.; Reyren, N.; Caviglia, A. D.; Fête, A.; Leake, S. J.; Pauli, S. A.; Willmott, P. R.; Stengel, M.; Ghosez, P.; Triscone, J. M. Electrostriction at the LaAlO3/SrTiO3 Interface. *Phys. Rev. Lett.* **2011**, *107*, 056102.
(18) Caviglia, A. D.; Gariglio, S.; Reyren, N.; Jaccard, D.; Schneider, T.; Gabay, M.; Thiel, S.; Hammerl, G.; Mannhart, J.; Triscone, J. M. Electric Field Control of the LaAlO3/SrTiO3 Interface Ground State. *Nature* **2008**, *456*, 624-627.
(19) Slooten, E.; Zhong, Z.; Molegraaf, H. J. A.; Eerkes, P. D.; de Jong, S.; Massee, F.; van Heumen, E.; Kruize, M. K.; Wenderich, S.; Kleibeuker, J. E.; Gorgoi, M.; Hilgenkamp, H.; Brinkman, A.; Huijben, M.; Rijnders, G.; Blank, D. H. A.; Koster, G.; Kelly, P. J.; Golden, M. S. Hard X-Ray Photoemission and Density Functional Theory Study of the Internal Electric Field in SrTiO3/LaAlO3 Oxide Heterostructures. *Phys. Rev. B* **2013**, *87*, 085128.
(20) Asmara, T. C.; Annadi, A.; Santoso, I.; Gogoi, P. K.; Kotlov, A.; Omer, H. M.; Motapothula, M.; Breese, M. B. H.; Rübhausen, M.; Venkatesan, T.; Ariando; Rusydi, A. Mechanisms of Charge Transfer and Redistribution in LaAlO3/SrTiO3 Revealed by High-Energy Optical Conductivity. *Nat. Commun.* **2014**, *5*, 3663.
(21) Yang, K.; Nazir, S.; Behtash, M.; Cheng, J. High-Throughput Design of Two-Dimensional Electron Gas Systems Based on Polar/Nonpolar Perovskite Oxide Heterostructures. *Sci. Rep.* **2016**, *6*, 34667.

(22) Huang, B.-C.; Chiu, Y.-P.; Huang, P.-C.; Wang, W.-C.; Tra, V. T.; Yang, J.-C.; He, Q.; Lin, J.-Y.; Chang, C.-S.; Chu, Y.-H. Mapping Band Alignment across Complex Oxide Heterointerfaces. *Phys. Rev. Lett.* **2012**, *109*, 246807.
(23) Segal, Y.; Ngai, J. H.; Reiner, J. W.; Walker, F. J.; Ahn, C. H. X-Ray Photoemission Studies of the Metal-Insulator Transition in LaAlO3/SrTiO3 Structures Grown by Molecular Beam Epitaxy. *Phys. Rev. B* **2009**, *80*, 241107.
(24) Wu, S.; Luo, X.; Turner, S.; Peng, H.; Lin, W.; Ding, J.; David, A.; Wang, B.; Van Tendeloo, G.; Wang, J.; Wu, T. Nonvolatile Resistive Switching in LaAlO3/SrTiO3 Heterostructures. *Phys. Rev. X* **2013**, *3*, 041027.
(25) Yu, L.; Zunger, A. A Polarity-Induced Defect Mechanism for Conductivity and Magnetism at Polar–Nonpolar Oxide Interfaces. *Nat. Commun.* **2014**, *5*.
(26) Zhou, J.; Asmara, T. C.; Yang, M.; Sawatzky, G. A.; Feng, Y. P.; Rusydi, A. Interplay of Electronic Reconstructions, Surface Oxygen Vacancies, and Lattice Distortions in Insulator-Metal Transition of LaAlO3/SrTiO3. *Phys. Rev. B* **2015**, *92*, 125423.
(27) Lee, P. W.; Singh, V. N.; Guo, G. Y.; Liu, H. J.; Lin, J. C.; Chu, Y. H.; Chen, C. H.; Chu, M. W. Hidden Lattice Instabilities as Origin of the Conductive Interface between Insulating LaAlO3 and SrTiO3. *Nat. Commun.* **2016**, *7*, 12773.
(28) Pentcheva, R.; Pickett, W. E. Avoiding the Polarization Catastrophe in LaAlO3 Overlayers on SrTiO3 (001) through Polar Distortion. *Phys. Rev. Lett.* **2009**, *102*, 107602.
(29) Sharma, P.; Ryu, S.; Burton, J. D.; Paudel, T. R.; Bark, C. W.; Huang, Z.; Ariando; Tsymbal, E. Y.; Catalan, G.; Eom, C. B.; Gruverman, A. Mechanical Tuning of LaAlO3/SrTiO3 Interface Conductivity. *Nano Lett.* **2015**, *15*, 3547-3551.
(30) Behtash, M.; Nazir, S.; Wang, Y.; Yang, K. Polarization Effects on the Interfacial Conductivity in LaAlO3/SrTiO3 Heterostructures: A First-Principles Study. *Phys. Chem. Chem. Phys.* **2016**, *18*, 6831-6838.
(31) Cao, Y.; Liu, X.; Shafer, P.; Middey, S.; Meyers, D.; Kareev, M.; Zhong, Z.; Kim, J.-W.; Ryan, P. J.; Arenholz, E.; Chakhalian, J. Anomalous Orbital Structure in a Spinel–Perovskite Interface. *npj Quantum Materials* **2016**, *1*, 16009.
(32) Siemons, W.; Koster, G.; Yamamoto, H.; Harrison, W. A.; Lucovsky, G.; Geballe, T. H.; Blank, D. H. A.; Beasley, M. R. Origin of Charge Density at LaAlO3 on SrTiO3 Heterointerfaces: Possibility of Intrinsic Doping. *Phys. Rev. Lett.* **2007**, *98*, 196802.
(33) Zhong, Z.; Xu, P. X.; Kelly, P. J. Polarity-Induced Oxygen Vacancies at LaAlO3/SrTiO3 Interfaces. *Phys. Rev. B* **2010**, *82*, 165127.
(34) Chen, Y. Z.; Bovet, N.; Trier, F.; Christensen, D. V.; Qu, F. M.; Andersen, N. H.; Kasama, T.; Zhang, W.; Giraud, R.; Dufouleur, J.; Jespersen, T. S.; Sun, J. R.; Smith, A.; Nygård, J.; Lu, L.; Büchner, B.; Shen, B. G.; Linderoth, S.; Pryds, N. A High-Mobility Two-Dimensional Electron Gas at the Spinel/Perovskite Interface of Γ-Al2o$_3$/SrTiO3. *Nat. Commun.* **2013**, *4*, 1371.
(35) David, A.; Tian, Y.; Yang, P.; Gao, X.; Lin, W.; Shah, A. B.; Zuo, J.-M.; Prellier, W.; Wu, T. Colossal Positive Magnetoresistance in Surface-Passivated Oxygen-Deficient Strontium Titanite. *Sci. Rep.* **2015**, *5*, 10255.
(36) Wang, L.; Dash, S.; Chang, L.; You, L.; Feng, Y.; He, X.; Jin, K.-j.; Zhou, Y.; Ong, H. G.; Ren, P.; Wang, S.; Chen, L.; Wang, J. Oxygen Vacancy Induced Room-Temperature Metal–Insulator Transition in Nickelate Films and Its Potential Application in Photovoltaics. *ACS Appl. Mater. Inter.* **2016**, *8*, 9769-9776.

(37) Kang, K. T.; Kang, H.; Park, J.; Suh, D.; Choi, W. S. Quantum Conductance Probing of Oxygen Vacancies in SrTiO3 Epitaxial Thin Film Using Graphene. *Adv. Mater.* **2017**, *29*, 1700071.
(38) Chen, Y.; Pryds, N.; Kleibeuker, J. E.; Koster, G.; Sun, J.; Stamate, E.; Shen, B.; Rijnders, G.; Linderoth, S. Metallic and Insulating Interfaces of Amorphous SrTiO3-Based Oxide Heterostructures. *Nano Lett.* **2011**, *11*, 3774-3778.
(39) Lee, S. W.; Liu, Y.; Heo, J.; Gordon, R. G. Creation and Control of Two-Dimensional Electron Gas Using Al-Based Amorphous Oxides/SrTiO3 Heterostructures Grown by Atomic Layer Deposition. *Nano Lett.* **2012**, *12*, 4775-4783.
(40) Willmott, P. R.; Pauli, S. A.; Herger, R.; Schlepütz, C. M.; Martoccia, D.; Patterson, B. D.; Delley, B.; Clarke, R.; Kumah, D.; Cionca, C.; Yacoby, Y. Structural Basis for the Conducting Interface between LaAlO3 and SrTiO3. *Phys. Rev. Lett.* **2007**, *99*, 155502.
(41) Kalabukhov, A. S.; Boikov, Y. A.; Serenkov, I. T.; Sakharov, V. I.; Popok, V. N.; Gunnarsson, R.; Börjesson, J.; Ljustina, N.; Olsson, E.; Winkler, D.; Claeson, T. Cationic Disorder and Phase Segregation in LaAlO3/SrTiO3 Heterointerfaces Evidenced by Medium-Energy Ion Spectroscopy. *Phys. Rev. Lett.* **2009**, *103*, 146101.
(42) Yamamoto, R.; Bell, C.; Hikita, Y.; Hwang, H. Y.; Nakamura, H.; Kimura, T.; Wakabayashi, Y. Structural Comparison of N-Type and P-Type LaAlO3/SrTiO3 Interfaces. *Phys. Rev. Lett.* **2011**, *107*, 036104.
(43) Biscaras, J.; Bergeal, N.; Kushwaha, A.; Wolf, T.; Rastogi, A.; Budhani, R. C.; Lesueur, J. Two-Dimensional Superconductivity at a Mott Insulator/Band Insulator Interface Latio$_3$/SrTiO3. *Nat. Commun.* **2010**, *1*, 89.
(44) Choi, W. S.; Lee, S. A.; You, J. H.; Lee, S.; Lee, H. N. Resonant Tunnelling in a Quantum Oxide Superlattice. *Nat. Commun.* **2015**, *6*, 7424.
(45) Annadi, A.; Putra, A.; Liu, Z. Q.; Wang, X.; Gopinadhan, K.; Huang, Z.; Dhar, S.; Venkatesan, T.; Ariando Electronic Correlation and Strain Effects at the Interfaces between Polar and Nonpolar Complex Oxides. *Phys. Rev. B* **2012**, *86*, 085450.
(46) Perna, P.; Maccariello, D.; Radovic, M.; Scotti di Uccio, U.; Pallecchi, I.; Codda, M.; Marré, D.; Cantoni, C.; Gazquez, J.; Varela, M.; Pennycook, S. J.; Granozio, F. M. Conducting Interfaces between Band Insulating Oxides: The Lagao$_3$/SrTiO3 Heterostructure. *Appl. Phys. Lett.* **2010**, *97*, 152111.
(47) Arras, R.; Calmels, L. Fully Spin-Polarized Two-Dimensional Electron Gas at the Cofe$_2$o$_4$/Mgal$_2$o$_4$ (001) Polar Interface. *Phys. Rev. B* **2014**, *90*, 045411.
(48) Boschker, H.; Verbeeck, J.; Egoavil, R.; Bals, S.; van Tendeloo, G.; Huijben, M.; Houwman, E. P.; Koster, G.; Blank, D. H. A.; Rijnders, G. Preventing the Reconstruction of the Polar Discontinuity at Oxide Heterointerfaces. *Adv. Funct. Mater.* **2012**, *22*, 2235-2240.
(49) Miura, Y.; Muramoto, S.; Abe, K.; Shirai, M. First-Principles Study of Tunneling Magnetoresistance in Fe/Mgal$_2$o$_4$/Fe(001) Magnetic Tunnel Junctions. *Phys. Rev. B* **2012**, *86*, 024426.
(50) Sukegawa, H.; Miura, Y.; Muramoto, S.; Mitani, S.; Niizeki, T.; Ohkubo, T.; Abe, K.; Shirai, M.; Inomata, K.; Hono, K. Enhanced Tunnel Magnetoresistance in a Spinel Oxide Barrier with Cation-Site Disorder. *Phys. Rev. B* **2012**, *86*, 184401.
(51) Li, W.-Z.; Kovarik, L.; Mei, D.; Liu, J.; Wang, Y.; Peden, C. H. F. Stable Platinum Nanoparticles on Specific Mgal$_2$o$_4$ Spinel Facets at High Temperatures in Oxidizing Atmospheres. *Nat. Commun.* **2013**, *4*, 2481.

(52) Schütz, P.; Pfaff, F.; Scheiderer, P.; Chen, Y. Z.; Pryds, N.; Gorgoi, M.; Sing, M.; Claessen, R. Band Bending and Alignment at the Spinel/Perovskite Γ-Al_2o_3/SrTiO3 Heterointerface. *Phys. Rev. B* **2015**, *91*, 165118.
(53) Yang, X.; Su, H.; Wu, G. Orbital-Adapted Electronic Structure and Anisotropic Transport in Γ-Al_2o_3/SrTiO3 Heterostructure. *Physical Review Materials* **2020**, *4*, 016001.
(54) Kresse, G.; Furthmüller, J. Efficient Iterative Schemes for Ab Initio Total-Energy Calculations Using a Plane-Wave Basis Set. *Phys. Rev. B* **1996**, *54*, 11169-11186.
(55) Kresse, G.; Furthmüller, J. Efficiency of Ab-Initio Total Energy Calculations for Metals and Semiconductors Using a Plane-Wave Basis Set. *Comp. Mater. Sci.* **1996**, *6*, 15-50.
(56) Blöchl, P. E. Projector Augmented-Wave Method. *Phys. Rev. B* **1994**, *50*, 17953-17979.
(57) Perdew, J. P.; Burke, K.; Ernzerhof, M. Generalized Gradient Approximation Made Simple. *Phys. Rev. Lett.* **1996**, *77*, 3865-3868.
(58) Sathiya, M.; Abakumov, A. M.; Foix, D.; Rousse, G.; Ramesha, K.; Saubanère, M.; Doublet, M. L.; Vezin, H.; Laisa, C. P.; Prakash, A. S.; Gonbeau, D.; VanTendeloo, G.; Tarascon, J. M. Origin of Voltage Decay in High-Capacity Layered Oxide Electrodes. *Nat. Mater.* **2014**, *14*, 230.
(59) Chambers, S. A.; Engelhard, M. H.; Shutthanandan, V.; Zhu, Z.; Droubay, T. C.; Qiao, L.; Sushko, P. V.; Feng, T.; Lee, H. D.; Gustafsson, T.; Garfunkel, E.; Shah, A. B.; Zuo, J. M.; Ramasse, Q. M. Instability, Intermixing and Electronic Structure at the Epitaxial LaAlO3/SrTiO3(001) Heterojunction. *Surf. Sci. Rep.* **2010**, *65*, 317-352.
(60) Kan, D.; Kanda, R.; Kanemitsu, Y.; Shimakawa, Y.; Takano, M.; Terashima, T.; Ishizumi, A. Blue Luminescence from Electron-Doped SrTiO3. *Appl. Phys. Lett.* **2006**, *88*, 191916.
(61) Daisuke, K.; Osami, S.; Shigeru, K.; Mikio, T.; Yuichi, S. Structural Characterization of Ar^+-Irradiated SrTiO3 Showing Room-Temperature Blue Luminescence. *Jpn. J. Appl. Phys.* **2007**, *46*, L471.
(62) Kan, D.; Terashima, T.; Kanda, R.; Masuno, A.; Tanaka, K.; Chu, S.; Kan, H.; Ishizumi, A.; Kanemitsu, Y.; Shimakawa, Y.; Takano, M. Blue-Light Emission at Room Temperature from Ar^+-Irradiated SrTiO3. *Nat. Mater.* **2005**, *4*, 816-819.
(63) Lee, S. A.; Jeong, H.; Woo, S.; Hwang, J.-Y.; Choi, S.-Y.; Kim, S.-D.; Choi, M.; Roh, S.; Yu, H.; Hwang, J.; Kim, S. W.; Choi, W. S. Phase Transitions Via Selective Elemental Vacancy Engineering in Complex Oxide Thin Films. *Sci. Rep.* **2016**, *6*, 23649.
(64) Zabaleta, J.; Borisov, V. S.; Wanke, R.; Jeschke, H. O.; Parks, S. C.; Baum, B.; Teker, A.; Harada, T.; Syassen, K.; Kopp, T.; Pavlenko, N.; Valentí, R.; Mannhart, J. Hydrostatic Pressure Response of an Oxide-Based Two-Dimensional Electron System. *Phys. Rev. B* **2016**, *93*, 235117.
(65) Li, Y.; Deng, R.; Lin, W.; Tian, Y.; Peng, H.; Yi, J.; Yao, B.; Wu, T. Electrostatic Tuning of Kondo Effect in a Rare-Earth-Doped Wide-Band-Gap Oxide. *Phys. Rev. B* **2013**, *87*, 155151.
(66) Caviglia, A. D.; Gabay, M.; Gariglio, S.; Reyren, N.; Cancellieri, C.; Triscone, J. M. Tunable Rashba Spin-Orbit Interaction at Oxide Interfaces. *Phys. Rev. Lett.* **2010**, *104*, 126803.
(67) Zhong, Z.; Tóth, A.; Held, K. Theory of Spin-Orbit Coupling at LaAlO3/SrTiO3 Interfaces and SrTiO3 Surfaces. *Phys. Rev. B* **2013**, *87*, 161102.
(68) Manchon, A.; Koo, H. C.; Nitta, J.; Frolov, S. M.; Duine, R. A. New Perspectives for Rashba Spin-Orbit Coupling. *Nat. Mater.* **2015**, *14*, 871-882.
(69) Nakamura, H.; Koga, T.; Kimura, T. Experimental Evidence of Cubic Rashba Effect in an Inversion-Symmetric Oxide. *Phys. Rev. Lett.* **2012**, *108*, 206601.
(70) Fête, A.; Gariglio, S.; Caviglia, A. D.; Triscone, J. M.; Gabay, M. Rashba Induced Magnetoconductance Oscillations in the LaAlO3-SrTiO3 Heterostructure. *Phys. Rev. B* **2012**, *86*, 201105.

(71) Lu, H.-Z.; Shen, S.-Q. Finite-Temperature Conductivity and Magnetoconductivity of Topological Insulators. *Phys. Rev. Lett.* **2014**, *112*, 146601.
(72) Reinle-Schmitt, M. L.; Cancellieri, C.; Li, D.; Fontaine, D.; Medarde, M.; Pomjakushina, E.; Schneider, C. W.; Gariglio, S.; Ghosez, P.; Triscone, J. M.; Willmott, P. R. Tunable Conductivity Threshold at Polar Oxide Interfaces. *Nat. Commun.* **2012**, *3*, 932.
(73) Breckenfeld, E.; Bronn, N.; Karthik, J.; Damodaran, A. R.; Lee, S.; Mason, N.; Martin, L. W. Effect of Growth Induced (Non)Stoichiometry on Interfacial Conductance in LaAlO3/SrTiO3. *Phys. Rev. Lett.* **2013**, *110*, 196804.
(74) Cen, C.; Thiel, S.; Hammerl, G.; Schneider, C. W.; Andersen, K. E.; Hellberg, C. S.; Mannhart, J.; Levy, J. Nanoscale Control of an Interfacial Metal-Insulator Transition at Room Temperature. *Nat. Mater.* **2008**, *7*, 298-302.
(75) Li, Y.; Phattalung, S. N.; Limpijumnong, S.; Kim, J.; Yu, J. Formation of Oxygen Vacancies and Charge Carriers Induced in the N-Type Interface of a LaAlO3 Overlayer on SrTiO3. *Phys. Rev. B* **2011**, *84*, 245307.
(76) Rebled, J. M.; Foerster, M.; Estradé, S.; Rigato, F.; Kanamadi, C.; Sánchez, F.; Peiró, F.; Fontcuberta, J. Ti Diffusion in (001) SrTiO3–$Cofe_2o_4$ Epitaxial Heterostructures: Blocking Role of a $Mgal_2o_4$ Buffer. *Phys. Chem. Chem. Phys.* **2013**, *15*, 18274-18280.
(77) Zheng, H.; Wang, J.; Lofland, S. E.; Ma, Z.; Mohaddes-Ardabili, L.; Zhao, T.; Salamanca-Riba, L.; Shinde, S. R.; Ogale, S. B.; Bai, F.; Viehland, D.; Jia, Y.; Schlom, D. G.; Wuttig, M.; Roytburd, A.; Ramesh, R. Multiferroic $Batio_3$-$Cofe_2o_4$ Nanostructures. *Science* **2004**, *303*, 661-663.